6th European Conference on Computational Mechanics (ECCM 6)
7th European Conference on Computational Fluid Dynamics (ECFD 7)
11 – 15 June 2018, Glasgow, UK

THE IC ENGINE COMBUSTION SIMULATION USING HIERARCHICAL CARTESIAN MESH FRAMEWORK

(ECCM –ECFD 2018 CONFERENCE)

WEI-HSIANG WANG[1], CHUNG-GUNG LI[2], RAHUL BALE[3], KEIJI ONISHI[4] AND MAKOTO TSUBOKURA[5, 6]

[1] RIKEN AICS
7 Chome-1-26 Minatojima Minamimachi, Chuo, Kobe, Hyogo, Japan
wei-hsiang.wang@riken.jp

[2] Kobe University
1-1 Rokkodaicho, Nada Ward, Kobe, Hyogo, Japan
cgli@aquamarine.kobe-u.ac.jp

[3] RIKEN AICS
7 Chome-1-26 Minatojima Minamimachi, Chuo, Kobe, Hyogo, Japan
rahul.bale@riken.jp

[4] RIKEN AICS
7 Chome-1-26 Minatojima Minamimachi, Chuo, Kobe, Hyogo, Japan
keiji.onishi@riken.jp

[5] RIKEN AICS
7 Chome-1-26 Minatojima Minamimachi, Chuo, Kobe, Hyogo, Japan
mtsubo@riken.jp

[6] Kobe University
1-1 Rokkodaicho, Nada, Kobe, Hyogo, Japan
tsubo@tiger.kobe-u.ac.jp

Key words: IC Engine, Combustion, Building Cube Method

Abstract. The IC engine is investigated numerically by Cartesian mesh system. The Building Cube Method is adopted to generate the mesh partition for complicated engine geometry and parallel computation. The fully compressible flow solver by Roe scheme and 5th order MUSCL is used to calculate the flow field with high pressure and temperature differences. The species transport equations are solved with 11 species of combustion in this framework. The chemical reaction of combustion is conducted by equilibrium solver of Cantera module, which is used for evaluate the equilibrium state of the reacting flow, and merged with the flow solver and G-equation flame front treatment. In order to simulate the engine motion, the geometry and engine moving piston is calculated by Immersed Boundary Method. The flow field of velocity, density and flame front due to the combustion and engine motion is shown in the results. The validation is done by the Rapid Compression Machine simulation with the comparison of experimental

data. The flame front shapes and flame propagation speed of this framework are well consistent with the experimental results.

1 INTRODUCTION

The subject of IC engine is very important for industrial application on automobile filed. The heat, mass and flow fields of combustion by the four-stroke procedure dominate the power and efficiency of the engine. The difficulty of this subject contains the complex geometry treatment of meshing and moving parts, the high compressibility of flow field and the chemical reactions of species including the transport phenomena. In this study, we built a CFD framework CUBE to solve this complicated IC engine simulation with Rapid Compression Machine (RCM) test. For the meshing system, the Cartesian grid by Building Cube Method [1] is adopted to avoid the hard work of unstructured meshing but still keep good resolution near engine wall. Due to the density difference of high compression ratio and the temperature difference of combustion, the fully compressible flow with species transport equations are solved by Roe scheme [2] and 5th order MUSCL scheme [3]. The chemical reaction calculation is imported from Cantera [4] module by equilibrium solver and merged with the flow solver with G-equation flame front treatment. Finally, the geometry and engine piston moving boundary are solved by the Immersed Boundary Method (IBM) [5]. The results showed reasonable flow fields and flame propagation with the experimental data.

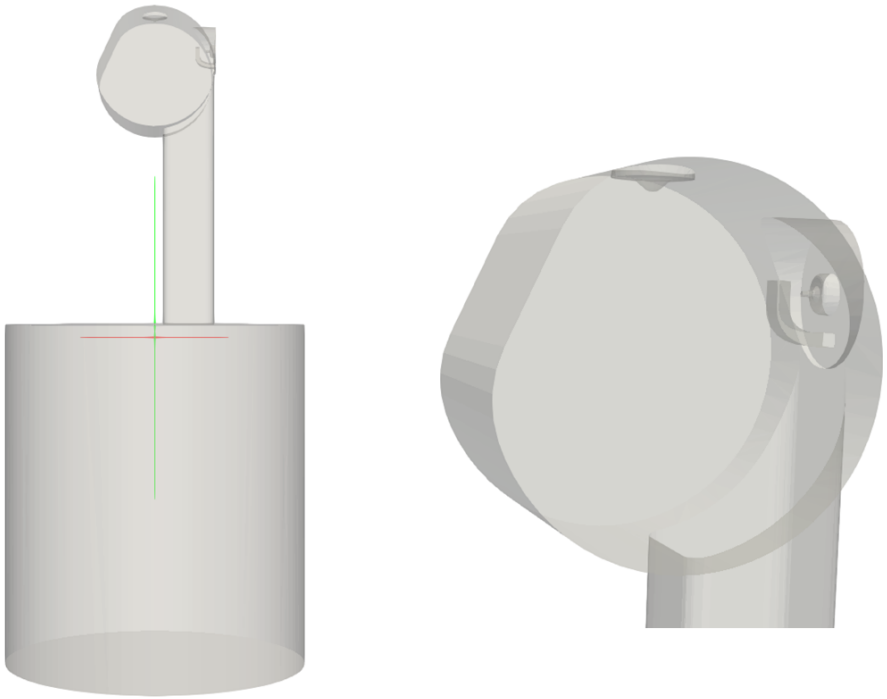

Figure 1: RCM geometry

2 PHYSICAL MODEL

The physical model of this study is a RCM as indicated in Figure 1(a). Figure 1(b) shows the detail spark plug and chamber geometry. Figure 2 shows the grid distribution, and the whole computation domain is divided by several cubes, and each cube contains 16×16×16 cells.

In this work, we discussed two conditions of RCM as listed in Table 1. Case A has an initial pressure of 200 kPa and with stationary piston at TDC, where case B is at 101.3 kPa of pressure and piston moves from BDC to TDC. Both cases are premix iso-octane/air and the equivalence ratio is equal to 1.0.

In order to simplify the chemical reaction calculation, only the main products of combustion are taken into account. The total species used in this study are iso-octane, O_2, H, O, OH, H_2O, H_2, CO, CO_2 , NO, and N_2. The gas properties are evaluated by the GRI-mechanism.

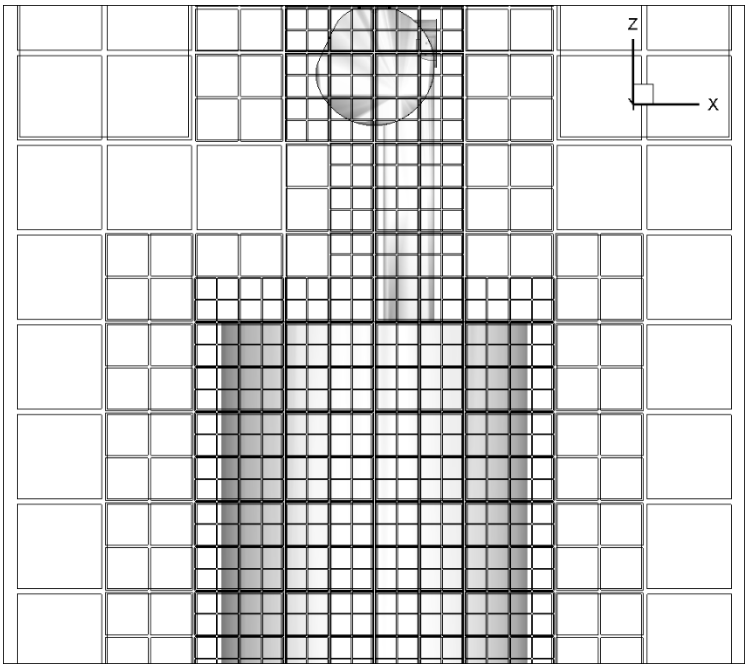

Figure 2: Cube distribution

Table 1: RCM conditions

	Fuel	Initial temperature(K)	Initial pressure(kPa)	Equivalence ratio	Ignition time	Compression ratio
Case A	Iso-octane	300	200	1.0	0ms	-
Case B	Iso-octane	300	101.3	1.0	80ms	13

3 NUMERICAL METHOD

In this paper, in order to solve the combustion phenomena in RCM, several methods are investigated. The Building Cube Method is adopted for the mesh distribution, and the

compressible flow with high temperature and pressure is solved by fully compressible flow solver. The transport phenomena of the fuel and reaction products and carrier gas are conducted by merging the species transport equations with compressible flow solver. For the flamelet model and combustion kinetics, the G equation solver and equilibrium module imported by Cantera are adopted.

3.1 Building Cube Method

The BCM [1] is used for mesh partition of RCM geometry. The whole computation domain is divided into several cubes, and each cube has the same numbers of uniform mesh grids, which is effective for parallel computation.

3.2 Fully compressible flow solver

In order to solve the fully compressible flow, the fifth-order differentiation for the derivative term of the MUSCL scheme is necessary. Besides, Roe scheme, preconditioning [6] are also adopted to solve the compressible governing equation as follows.

$$\frac{\partial U}{\partial t}+\frac{\partial F}{\partial x}+\frac{\partial G}{\partial y}+\frac{\partial H}{\partial z}=S \tag{1}$$

U and F are described as follows.

$$U=\begin{pmatrix}\rho\\ \rho u\\ \rho v\\ \rho w\\ \rho E\end{pmatrix}\quad F_i=\begin{pmatrix}\rho u\\ \rho u^2+P\\ \rho uv\\ \rho uw\\ \rho Eu+Pu\end{pmatrix}\quad F_v=\begin{pmatrix}0\\ -\tau_{xx}\\ -\tau_{xy}\\ -\tau_{xz}\\ q_x-u\tau_{xx}-v\tau_{xy}-w\tau_{xz}\end{pmatrix} \tag{2}$$

F_i is the inviscid term solved by Roe scheme and 5th order MUSCL, where F_v is the viscous term solved by 2nd order central difference. G and H are as the same expressionas as F for y and z directions.

3.3 Species transport equations and G equation

The species transport equations and G equation are merged and coupled with compressible flow governing equations with additional 11 equations for species and 1 equation for G. The final expression of governing equations are as follows.

$$U=\begin{pmatrix}\rho\\ \rho u\\ \rho v\\ \rho w\\ \rho E\\ \rho Y_1\\ \vdots\\ \rho Y_{11}\\ \rho G\end{pmatrix}\quad F_i=\begin{pmatrix}\rho u\\ \rho u^2+P\\ \rho uv\\ \rho uw\\ \rho Eu+Pu\\ \rho uY_1\\ \vdots\\ \rho uY_{11}\\ \rho uG\end{pmatrix}\quad F_v=\begin{pmatrix}0\\ -\tau_{xx}\\ -\tau_{xy}\\ -\tau_{xz}\\ q_x-u\tau_{xx}-v\tau_{xy}-w\tau_{xz}\\ \rho\hat{u}_1Y_1\\ \vdots\\ \rho\hat{u}_{11}Y_{11}\\ 0\end{pmatrix} \tag{3}$$

where

$$q_x=-k\frac{\partial T}{\partial x}+\rho\sum_{i=1}^{N}\bar{h}_i\hat{u}_iY_i \tag{4}$$

and

$$\hat{u}_iY_i=-D_{im}\frac{\partial Y_i}{\partial x} \tag{5}$$

$\bar{h}_i$, $\hat{u}_i$, Y_i, and D_{im} are the mass enthalpy, diffusion velocity, mass fraction and diffusion coefficient of ith species, respectively.

In G equation, there is a source term of $S_L|\nabla G|$, which indicates the effects of flame speed in combustion. This flame speed is estimated by the correlation equation of Metghalchi and Keck [7] as follows.

$$S_L=S_{u0}\left(\frac{T_u^0}{T_0}\right)^{\alpha}\left(\frac{p}{p_0}\right)^{\beta}(1-2.1f) \tag{6}$$

where

$$\begin{aligned}S_{uo}&=B_m+B_2(\phi-\phi_m)^2\\ \alpha&=2.18-0.8(\phi-1)\\ \beta&=-0.16+0.22(\phi-1)\\ T_0&=298K\\ P_0&=1\text{atm}\end{aligned}$$

and B_m, B_2 and ϕ_m are fuel constant parameters from [7].

3.4 Re-initialization of G equation

Since G equation is solved by level set function, the characteristic of it may be destroyed during the calculation. Therefore, a re-initialization procedure is performed ones every several timesteps. The values of G near flame front is iterated and reconstructed to $|\nabla G| = 1$ by the smoothed sign function as follows.

$$\frac{\partial G_n}{\partial \tau} + SG_0(|\nabla G_n| - 1) = 0 \tag{7}$$

$$SG_0 = \frac{G_0}{\sqrt{G_0^2 + \varepsilon^2}} \tag{8}$$

where SG_0 is the smoothed function of G equation and G_0 is the solution of G equation.

3.4 Cantera equilibrium module

For simplifying the chemical reaction calculation, the equilibrium model is used from the Cantera module. When the flame front solved by G equation moves to the unburned cell, the state of this cell will become a burned cell, and the chemical species will be also changed with heat released as a source term. The whole framework is shown in Figure 3.

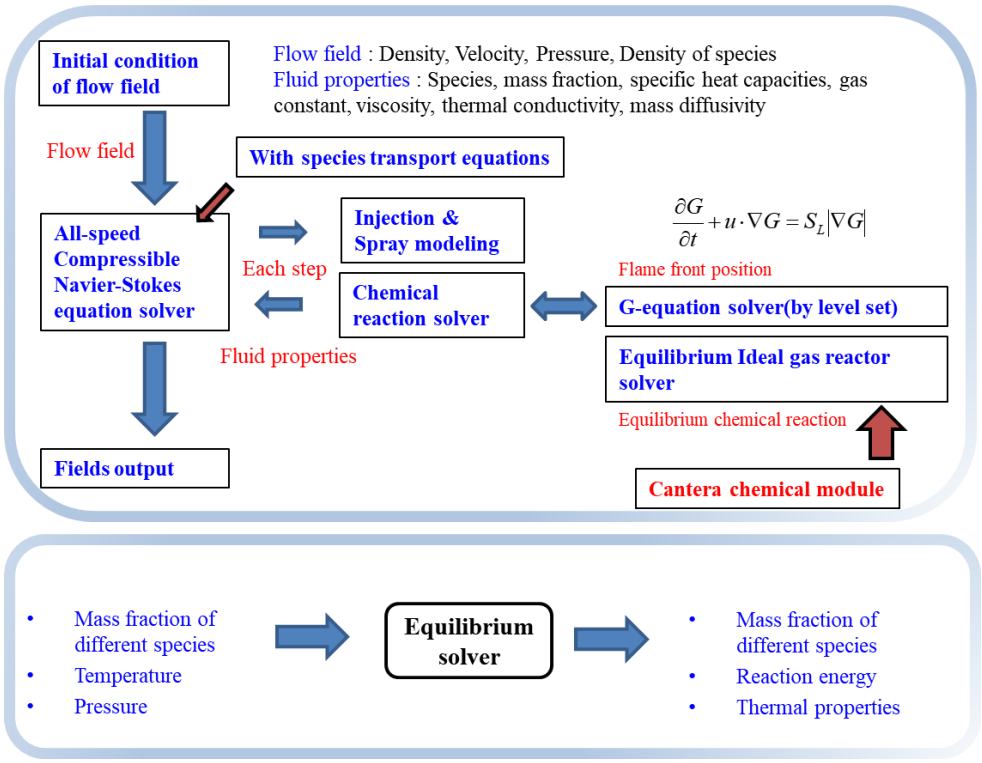

Figure 3: Engine simulation framework

4 RESULTS AND DISCUSSION

4.1 Computation parameters

In case A, the computation domain contains only the region of upper chamber above TDC, where in case B the whole domain is calculated. The total grid number of case A is around 5M and for case B is around 24M, both with a minimum cell size equals to 0.4mm near wall as shown in figure 2.

Since the fully compressible flow solver is adopted in this study, according to the CFL number we can decide the time step size that $\Delta t \le CFL \times \Delta x / c$. To make the simulation stable, usually the $CFL = 0.3$ is chosen, and c is the speed of sound. However, in combustion simulation, the speed of sound is not constant and varied with temperature by the expression of $c = \sqrt{\gamma RT}$, where γ is the specific heat ratio and R is the gas constant. For the combustion of iso-octane/air with equivalence ratio equals to 1.0, the temperature will be increased to about 3000K and makes the speed of sound also be increased to three times compared with ambient temperature($\cong 300K$). Finally, the time step size of $\Delta t = 1.25 \times 10^{-7}$ is chosen for the combustion part.

In case B, the piston is moving from BDC to TDC, and then the ignition and combustion are started. In this situation, for the computation before combustion, the species transport equations and G equation are not necessary, and can be removed from the governing equations to reduce the computation cost. Besides, the time step size before combustion can be also increased to $\Delta t = 2.5 \times 10^{-7}$ since the temperature is not increased so much.

The total physical time for case A is 0.03s and for case B is 0.1s. The total time steps for case A is 240000 steps and for case B is 320000(without combustion) plus 160000(with combustion) steps.

4.2 Premixed combustion without piston motion

In case A, the premixed combustion without piston motion is investigated. The fluids near the spark plug are heated and burned. Figure 4 shows the flame propagation with time. The iso-surface is define by $G = 0$, which is the flame front position, and the color is contoured by density.

Since the expansion phenomena, which is due to the high pressure and temperature of burning fluids, dominate the flow fields in this case, the flame shape is nearly like a sphere at initial stage, and then expanded and affected by the spark plug and the wall of chamber. As the flame propagates, the unburned fluids are pushed and compressed then makes the density of them getting higher and higher. As a result, the flame speed is higher at initial and getting lower with the propagation of the flame front.

Figure 5 shows the comparison of CFD results and experimental snapshots. The flame shape and flame speed of CFD are well consistent with the snapshots of experiments at almost every time step even for those wrinkles at the tip of flames. However, since the ignition condition is difficult to represent perfectly at the initial stage, there is a small difference between CFD and experimental results when ignition occurred.

4.3 Premixed combustion with piston motion

Case B shows the premixed combustion with piston motion. From $t = 0$ to $t = 80ms$, the piston moves from BDC to TDC as shown in figure 6. The density is increased due to the

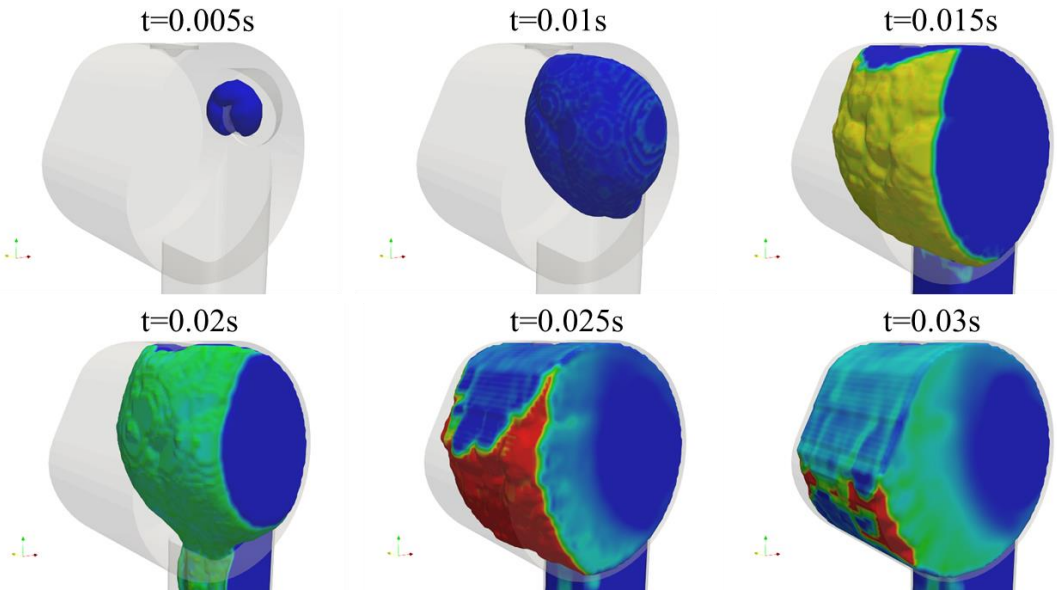

Figure 4: Distribution of flamefront with time of case A

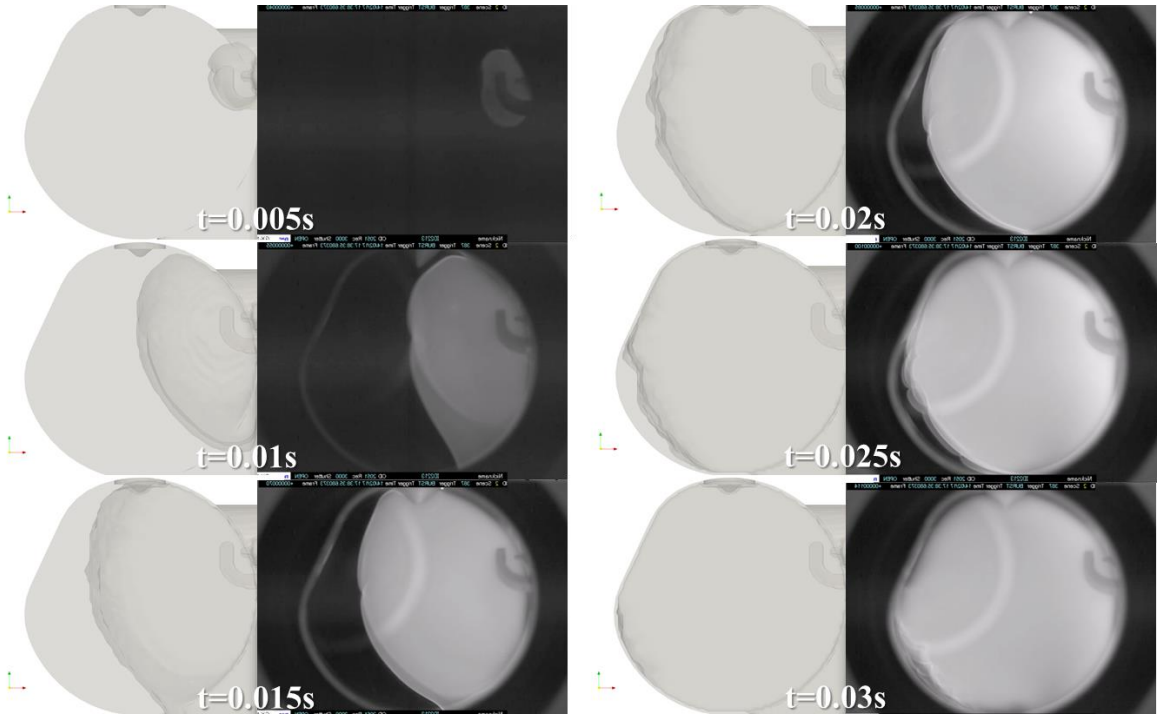

Figure 5: The comparison of flamefront of CFD (left) and experiments (right) with time of case A

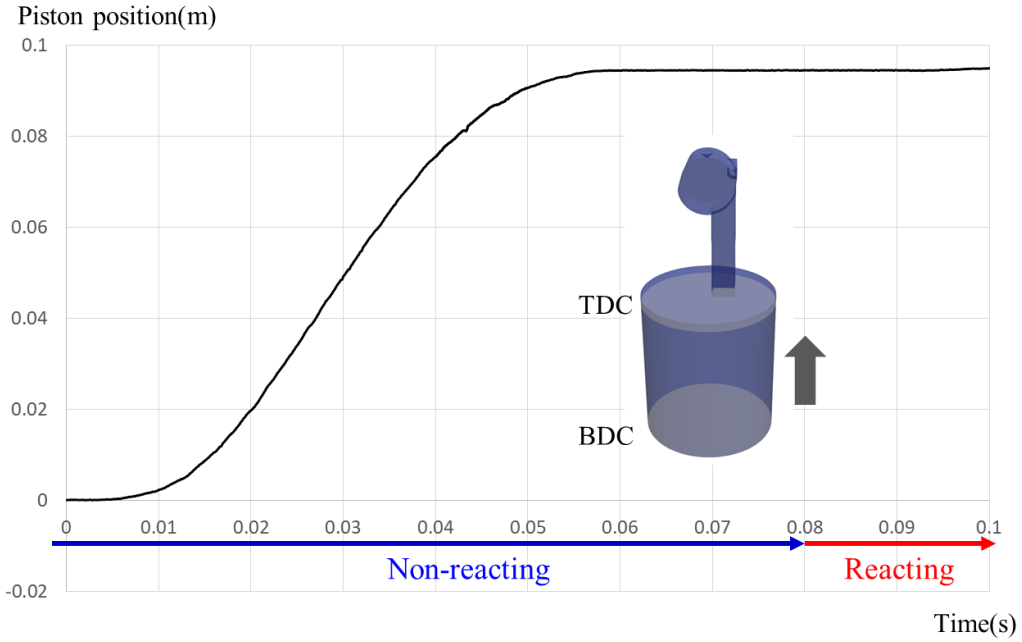

Figure 6: Piston motion of case B

compression process and is shown in figure 7. In figure 8, as the piston moving, the momentum magnitude inside the chamber is increased and even higher than the piston speed due to the geometry of the neck of the chamber. It makes the flow condition much more different and complicated than case A.

Figure 9 shows the comparison of pressure between experimental and CFD results. The pressure measurement point is indicated as the blue point inside the chamber as shown in the figure. Both results showed that the pressure is increased as the piston going to the TDC, and dramatically raised after 80ms due to the ignition. Before 40ms, the CFD results are well consistent with the experimental results, but has discrepancy after that. It is due to the insufficient mesh resolution inside the chamber. The moving geometry is solved by IBM in this study, which means the mesh distribution is kept the same position and size during the piston moving. When the piston moves from BDC to TDC, the resolution inside the chamber near piston is getting lower and lower and finally cannot well resolve the results. It is a weak point of IBM, but can be solved by locally increasing the resolution near that area.

In figure 10, the flamefront visualization results of CFD are compared with experimental snapshots. Due to the shape of the combustion chamber, the flamefront appears near the spark plug at beginning, and then counterclockwise moves through upper part and finally propagates to the whole chamber. The flame propagation speed and trends of CFD are similar to the experimental results though the full consistency is difficult to show because there are overlap flames inside the chamber.

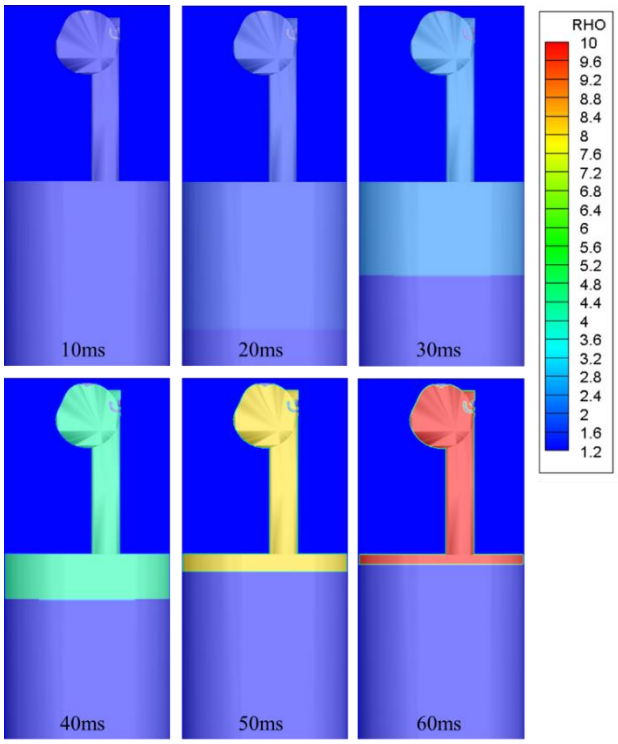

Figure 7: Density contours of slice at $y = 0$ of case B

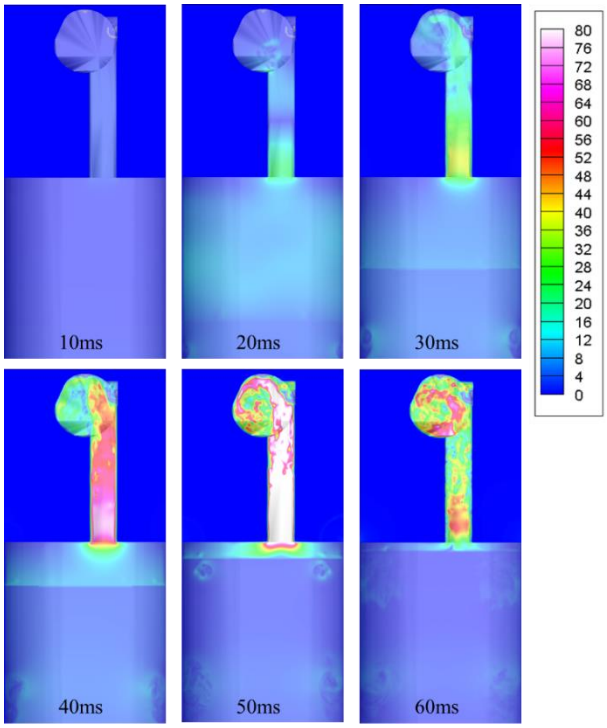

Figure 8: Momentum magnitude contours of slice at $y = 0$ of case B

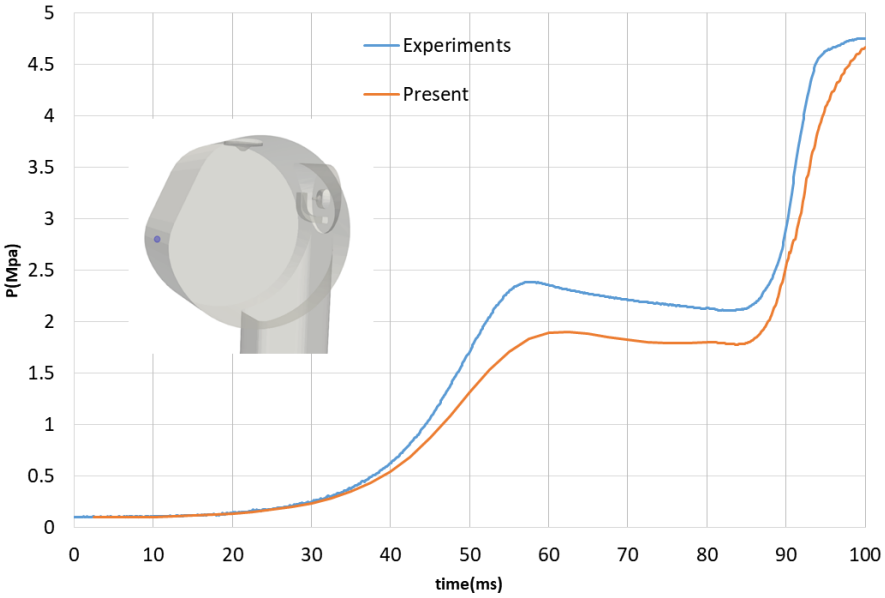

Figure 9: Pressure variations of experimental and CFD results of case B

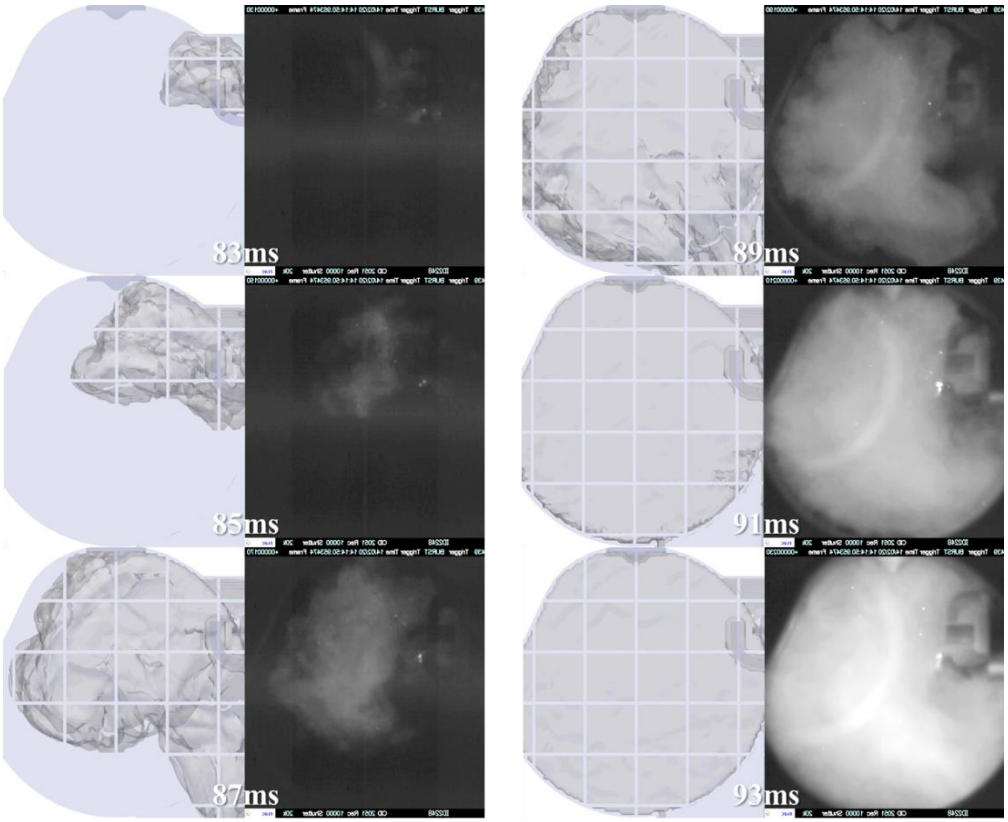

Figure 10: The comparison of flamefront of CFD (left) and experiments (right) of case B

5 CONCLUSIONS

- The IC engine is investigated numerically by Cartesian mesh system with fully compressible flow and combustion solver and Immersed Boundary Method. The species transport equations and G equation are solved for the mass fractions of combustion fuel and products as well as the flame front position.
- The validations are carried out by without and with moving piston in the RCM tests. Both results showed good agreements with experimental data of flame propagation speed and flame patterns.

ACKNOWLEDGMENT

The authors gratefully acknowledge the support of Mazda Motor Corporation for providing the experimental data of RCM.

REFERENCES

[1] Nakahashi, K. *Building-Cube Method for Flow Problems with Broadband Characteristic Length*. Comput. Fluid Dynamics (2002): 77-81.

[2] Roe, P.L. *Approximation Riemann solver, Parameter Vectors, and Difference Schemes*. J. Comput. Phys. (1981) **43**:357-372.

[3] Abalakin, I, Dervieux, A. and Kozubskaya, T. *A vertex centered high order MUSCL scheme applying to linearized Euler acoustics*, INRIA (2002): 4459.

[4] Goodwin, D.G., Moffat, H.K. and Speth, R.L. *Cantera: An object- oriented software toolkit for chemical kinetics, thermodynamics, and transport processes*. http://www.cantera.org (2017): Version 2.3.0.

[5] Li, C.G., Tsubokura M. and Bale, R. *Framework for simulation of natural convection in practical applications*. Int. Commun. Heat Mass Transf. (2016) **75**:52-58.

[6] Weiss J. M. and Simth, W. A. *Preconditioning Applied to Variable and Constants Density Flows*. AIAA (1995) **33**:2050-2056.

[7] Metghalchi, M. and Keck, J.C. *Burning Velocities of Mixtures of Air with Methanol, Isooctane, and Indolene at High Pressure and Temperature*. Combust. Flame. (1982) **48**:191-210.